Astronomy & Astrophysics

Spatially resolved spectroscopy of Coma cluster early-type galaxies

II. The minor axis dataset[*]

G. Wegner[1],[**], E. M. Corsini[2], R. P. Saglia[3,4], R. Bender[3,4], D. Merkl[3,5], D. Thomas[3,4], J. Thomas[3], and D. Mehlert[6]

[1] Department of Physics and Astronomy, 6127 Wilder Laboratory, Dartmouth College, Hanover, NH 03755-3528, USA

[2] Dipartimento di Astronomia, Università di Padova, Vicolo dell'Osservatorio 2, 35122 Padova, Italy

[3] Universitätssternwarte München, Scheinerstraße 1, 81679 München, Germany

[4] Max-Planck-Institut für extraterrestrische Physik, Postfach 1312, 85741 Garching, Germany

[5] Max-Planck-Institut für Plasmaphysik, Boltzmannstraße 2, 85748 Garching, Germany

[6] Landessternwarte Heidelberg, Königstuhl, 69117 Heidelberg, Germany

Abstract. We present minor axis, offset major axis and one diagonal long slit spectra for 10 E and S0 galaxies of the Coma cluster drawn from a magnitude-limited sample studied before. We derive rotation curves, velocity dispersion profiles and the H_3 and H_4 coefficients of the Hermite decomposition of the line of sight velocity distribution. Moreover, we derive the line index profiles of Mg, Fe and Hβ line indices and assess their errors. The data will be used to construct dynamical models of the galaxies and study their stellar populations.

Key words. galaxies: elliptical and lenticular, cD – galaxies: kinematics and dynamics – galaxies: stellar content – galaxies: abundances – galaxies: formation

1. Introduction

This is the second of a series of papers aimed at investigating the stellar populations and the dynamics of early-type galaxies in the Coma Cluster. Spanning about 4 dex in density, the Coma cluster is the ideal place to investigate these galaxy properties as a function of the environmental density. In the first paper of the series (Mehlert et al. 2000, hereafter Paper I) we presented the galaxy sample, its selection properties, the photometric observations and the long-slit major axis spectra for 35 E and S0 galaxies of the Coma Cluster. Here we complement the spectroscopic database with minor axis, offset major axis and one diagonal long slit spectra for 10 objects of the sample. The combined dataset allows the construction of dynamical axisymmetric models of the objects, to study the properties of the dark matter halos of flattened, rotating E and S0 galaxies. This study

is complementary to the one presented by Gerhard et al. (2001), focusing on round, non-rotating ellipticals.

The properties of the stellar populations of the central regions of Coma cluster galaxies have been investigated in detail by means of long-slit (Davies et al. 1987; Jørgensen et al. 1995; Lucey et al. 1997) and fibre-fed spectrographs (Jørgensen 1999; Mobasher et al. 2001; Poggianti et al. 2001a, b; Komiyama et al. 2002; Carter et al. 2002). The data presented here and in Paper I allow the study of the stellar population gradients for a restricted number of galaxies and the empirical verification of the aperture corrections (Jørgensen et al. 1995). Morover, possible systematic differences between the disk and bulge components of S0 galaxies can be investigated.

The spectroscopic observations and data reduction are described in Sect. 2. We present the derived kinematics in Sect. 3 and the line indices in Sect. 4. Conclusions are drawn in Sect. 5.

2. Observations and data reduction

2.1. Galaxy sample

All the observed galaxies (Table 1) belong to sample of 35 E and S0 galaxies of the Coma cluster studied in Paper I).

Table 1. Log of spectroscopic observations.

Object	Run	PA [°]	Position	Offset ["]	Single Exp. Time [s]	Total Exp. Time [h]	Q
(1)	(2)	(3)	(4)	(5)	(6)	(7)	(8)
GMP 0144	4	1	MN	-	$5 \times 3600 + 1776$	5.5	3
GMP 0282	3	135	MN	-	3×3600	3.0	2
GMP 0756	3	88	‖ MJ	5.8 N	6×3600	6.0	3
	3	178	MN	-	3×4200	3.5	2
GMP 1176	1	78	MJ	-	3×1800	1.5	2
	1	78	‖ MJ	2.6 N	5×3600	5.0	3
	1	168	MN	-	4×3600	4.0	1
GMP 1750	1	150	MN	-	3×3600	3.0	1
GMP 1990	1	135	‖ MJ	3.5 N	6×3600	6.0	2
	1-2	45	MN	-	3×3600	3.0	2
GMP 3510	2	79	MN	-	2×4200	2.3	2
GMP 3792	1	127	MJ	-	3×1800	1.5	2
	4	127	MJ	-	3×1800	1.5	3
	1	37	MN	-	3×4200	3.5	1
GMP 3818	3	127	DG	-	3×1800	1.5	3
GMP 5975	4	113	MN	-	3×3600	3.0	3

Column 1: GMP No. from Godwin, Metcalfe & Peach (1983). Column 2: observing run. Column 3: slit position angle measured North through East. Column 4: slit position. MJ = major axis; ‖ MJ = parallel to major axis; MN = minor axis; DG = diagonal axis. Column 5: northward offset of the slit with respect to galaxy center. Column 6: number and exposure time of the single exposures. Column 7: total exposure time. Column 8: estimated quality of the resulting spectrum. 1: very good; 2: good; 3: medium (see Fig. 1).

For details about their morphological classification and relevant photometric properties (i.e. total magnitude, effective radius, mean surface brightness within effective radius, ellipticity at effective radius and luminosity weighted a_4 parameter) the reader is referred to that paper. They were selected from the sample of Paper I as the objects with the most extended and precise major axis kinematics and therefore best suited for dynamical modelling, balancing the number of E and S0 types.

2.2. Long-slit spectroscopy

Long-slit spectroscopic data of the sample galaxies were obtained with the 2.4-m Hiltner telescope of the MDM Observatory at Kitt Peak, Arizona, USA, during four different runs between 1999 and 2001. Details of the instrumental set-up of the observations carried out on 16–20 April 1999 (run 1), 23–26 April 1999 (run 2), 26–30 May 2000 (run 3) and 9–12 February 2001 (run 4) are given in Table 2.

Minor-axis spectra were obtained for all the sample galaxies, while offset spectra with the slit parallel to the major axis were obtained only for GMP 0756, GMP 1176, GMP 1990. GMP 3818 was observed along a diagonal axis. In addition, we took spectra of GMP 1176 and GMP 3792 along their major axes to perform a consistency check with measurements of kinematics and line strength indices of Paper I. The typical

Table 2. Instrumental set-up of spectroscopic observations.

Parameter	Run 1-2	Run 3-4
Spectrograph	Modular	Modular
Grating	1200 gr mm^{-1}	1200 gr mm^{-1}
CCD	"Charlotte" SITe	"Echelle" SITe
Pixel number	1024×1024	2048×2048
Pixel size	$24 \times 24\ \mu m^2$	$24 \times 24\ \mu m^2$
Gain	3.2 e^-ADU^{-1}	2.7 e^-ADU^{-1}
RON	5.5 e^-	7.9 e^-
Scale	0.″606 pixel^{-1}	0.″606 pixel^{-1}
Dispersion	1.20 Å pixel^{-1}	1.01 Å pixel^{-1}
Slit width	2.″0	1.″9
Wavelength range	4916–5881 Å	4585–6470 Å
Instrumental $FWHM$	3.20 Å	3.11 Å
Instrumental σ[a]	79 km s^{-1}	77 km s^{-1}
Seeing $FWHM$	1.″9–3.″0	2.″0–3.″0

[a] Derived at the 5170 Å Mg triplet.

integration time of the galaxy spectra was 3600 s. Total integration times and slit position angle of the galaxy spectra as

well as the log of the spectroscopic observations are given in Table 1. At the beginning of each exposure the galaxy was centered on the slit using the guiding camera. In each run several spectra of giant stars with spectral type ranging from late-G to early-K were obtained to be used as templates in measuring stellar kinematics and line strength indices. The template stars were selected from Faber et al. (1985) and González (1993). Additionally we observed at least one flux standard star per night to calibrate the flux of the spectra before the line indices were measured. Spectra of the comparison Hg-Ne-Ar-Xe arc lamp were taken before and/or after object exposures to allow an accurate wavelength calibration. The value of the seeing $FWHM$ during the observing run as measured by fitting a two-dimensional Gaussian to the guide star is given in Table 2.

2.3. Basic data reduction

All the spectra were bias subtracted, flatfield corrected, cleaned of cosmic rays, corrected for bad columns and wavelength calibrated using standard MIDAS[1] routines. The flatfield correction was performed by means of both quartz lamp and twilight sky spectra, which were normalized and divided into all the spectra, to correct for pixel-to-pixel sensitivity variations and large-scale illumination patterns due to slit vignetting. Cosmic rays were identified and eliminated by interpolating over as in Bender et al. (1994, BSG94 hereafter). The residual cosmic rays were eliminated by manually editing the spectra. The wavelength calibration was performed by means of the MIDAS package XLONG. Each spectrum was rebinned using the wavelength solution obtained from the corresponding arc-lamp spectrum. We checked that the wavelength rebinning had been done properly by measuring the difference between the measured and predicted wavelengths (Osterbrock et al. 1996) for the brightest night-sky emission lines in the observed spectral range. The resulting accuracy in the wavelength calibration is ~0.08 Å corresponding to ~5 km s^{-1} at 5170 Å. The instrumental resolution was derived as the mean of the Gaussian $FWHMs$ measured for a number of unblended arc-lamp lines which were distributed over the whole spectral range of a wavelength-calibrated spectrum. The mean $FWHM$ of the arc-lamp lines and the corresponding instrumental resolution derived at 5170 Å is given in Table 2. In the galaxy and the stellar spectra the contribution of the sky was determined by interpolating along the outermost 10″−20″ at the two edges of the slit, where the galaxy or stellar light was negligible, and then subtracted. A sky subtraction better than 1% was achieved. All the spectra were corrected for CCD misalignment following BSG94. The spectra obtained for the same galaxy along the same axis were coadded using the center of the stellar continuum as a reference. This allowed to improve the signal-to-noise ratio (S/N) of the resulting two-dimensional spectrum. A one-dimensional spectrum was obtained for each kinematical template star as well as for each flux standard star. The spectra of the kinematical Lick-system templates were deredshifted to laboratory wavelengths.
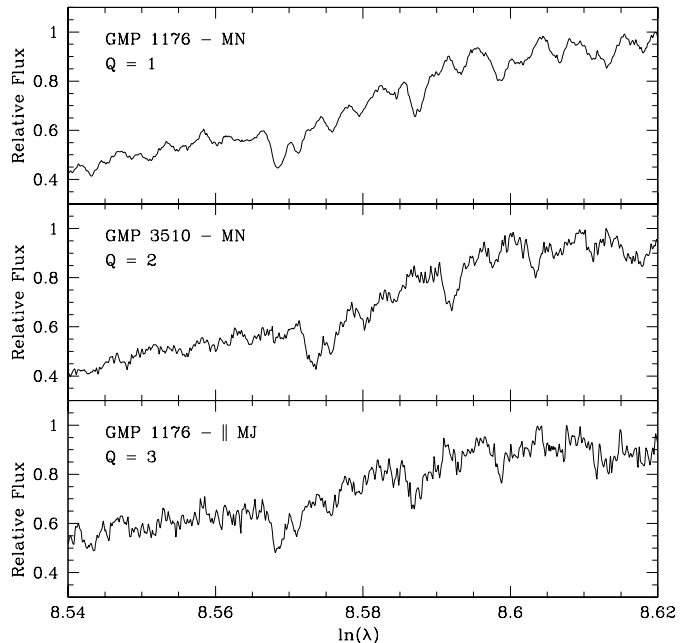
Fig. 1. Examples of central spectra covering the range of quality classes. Relative fluxes have false zero points for viewing convenience.

3. Stellar kinematics

We measured the stellar kinematics from the galaxy absorption features present in the wavelength range and centered on the Mg line triplet ($\lambda\lambda$ 5164, 5173, 5184 Å) by applying the Fourier Correlation Quotient method (Bender 1990) as done by BSG94.

The spectra were rebinned along the dispersion direction to a natural logarithmic scale, and along the spatial direction to obtain a nearly constant $S/N \geq 20$ per resolution element. In a few spectra the S/N decreases to ~10 at the outermost radii. The galaxy continuum was removed row-by-row by fitting a fourth to sixth order polynomial. The quality of the final spectrum depends on the resulting S/N. In Fig. 1 we show examples of central spectra covering the 3 quality classes listed in Table 1. The quality parameter is 1 for $S/N \geq 100$, 2 for $50 \leq S/N < 100$, 3 for $20 < S/N < 50$.

To measure the stellar kinematics of the sample galaxies we adopted HR 6817 (K1III) as kinematical template for runs 1, 2 and 3 and HR 3427 (K0III) for run 4 and we considered the wavelength range 5115–5541 Å (see Fig. 1) around the Mg lines of the galaxies. We derived for each galaxy spectrum the line-of-sight velocity distribution (LOSVD) along the slit and measured its moments, namely the radial velocity v, the velocity dispersion σ and the values of the coefficients H_3 and H_4. At each radius, they have been derived by fitting the LOSVD with a Gaussian plus third- and fourth-order Gauss-Hermite polynomials $\mathcal{H}_3$ and $\mathcal{H}_4$, which describe the asymmetric and symmetric deviations of the LOSVD from a pure Gaussian profile (van der Marel & Franx 1993; Gerhard 1993). Errors on the LOSVD moments were derived from photon statistics and CCD read-out noise, calibrating them by Monte Carlo simulations as done by BSG94. In general, errors are in the range
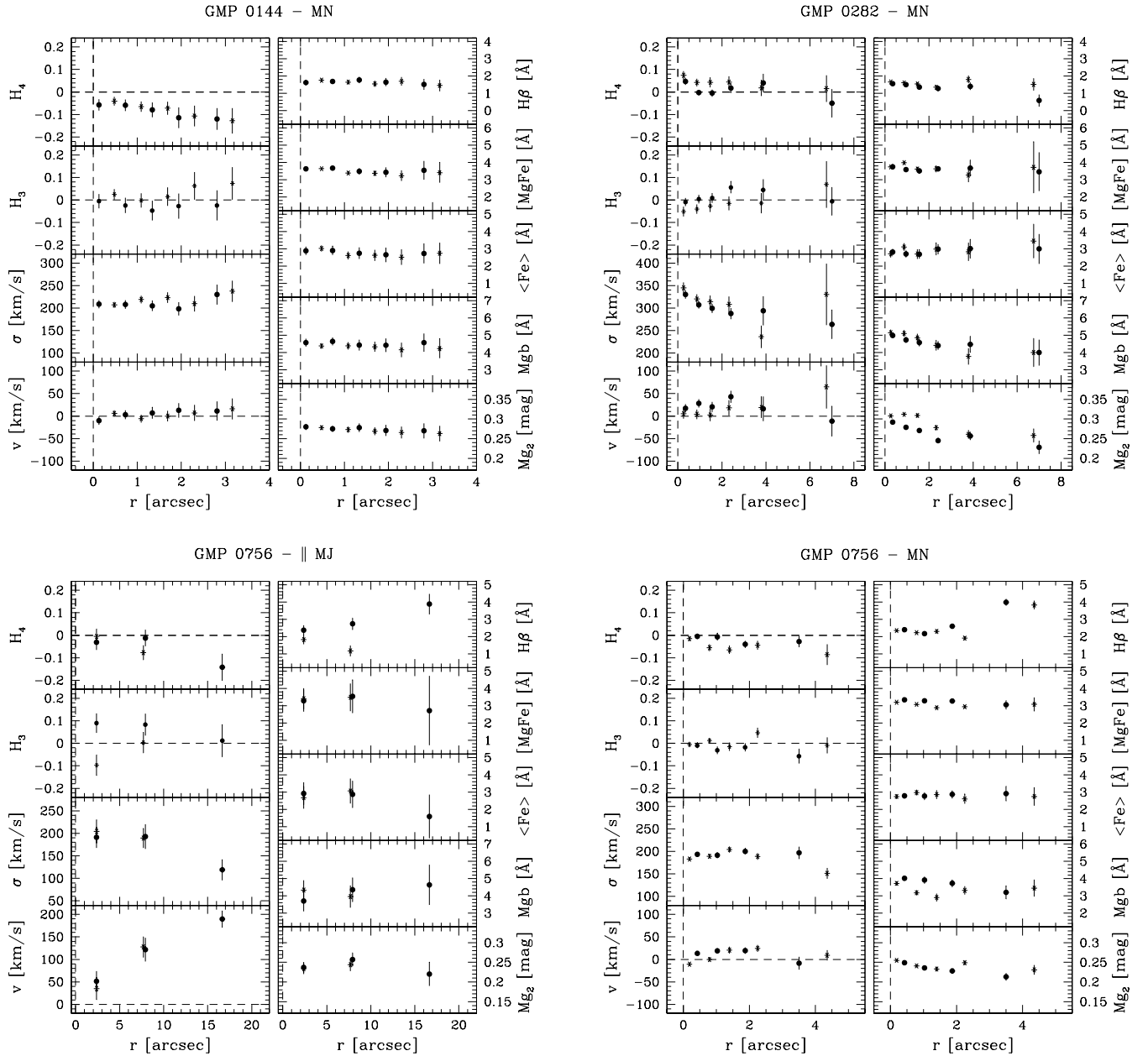
Fig. 2. Kinematical parameters and line indices measured along the observed axes of the sample galaxies. For each axis the curves are folded around the nucleus and filled dots and asterisks refer to the two sides of the galaxy. The radial profiles of the line-of-sight velocity (v) after the subtraction of systemic velocity, velocity dispersion (σ), third (H_3) and fourth (H_4) order coefficient of the Gauss-Hermite decomposition of the LOSVD are shown in the left panels (from top to bottom). The radial profiles of the line indices Hβ, [MgFe], <Fe>, Mgb and Mg$_2$ are plotted in the right panels (from top to bottom).

of 3–10 km s^{-1} for v and σ, and of 0.01–0.04 for H_3 and H_4, becoming larger in the outer parts of some galaxies where for $10 \leq S/N < 20$. These errors do not take into account possible systematic effects due to template mismatch or the presence of dust and/or faint emission. The measured stellar kinematics are reported in Table 3 and plotted in Fig. 2.

Figure 3 shows the comparison between the measurements of v, σ, H_3, and H_4 along the major axis of GMP 1176 and GMP 3792 obtained here and measurements obtained in Paper I. The value derived from the different datasets are in agreement within the errors. However in the case of GMP 3792

the velocity dispersion measured in run 4 is systematically lower than that measured both in Paper I and in run 1.

4. Line indices

We measured the Mg, Fe, and Hβ line strength indices following Worthey et al. (1994) from flux calibrated spectra, as done in Paper I. Spectra were rebinned in the dispersion direction as well as in the radial direction as before. We indicate the average Iron index with <Fe> = (Fe$_{5270}$ + Fe$_{5335}$)/2 (Gorgas et al. 1990) and the usual combined Magnesium-Iron index with [MgFe] = $\sqrt{\text{Mg}b < \text{Fe} >}$ (González 1993). We corrected
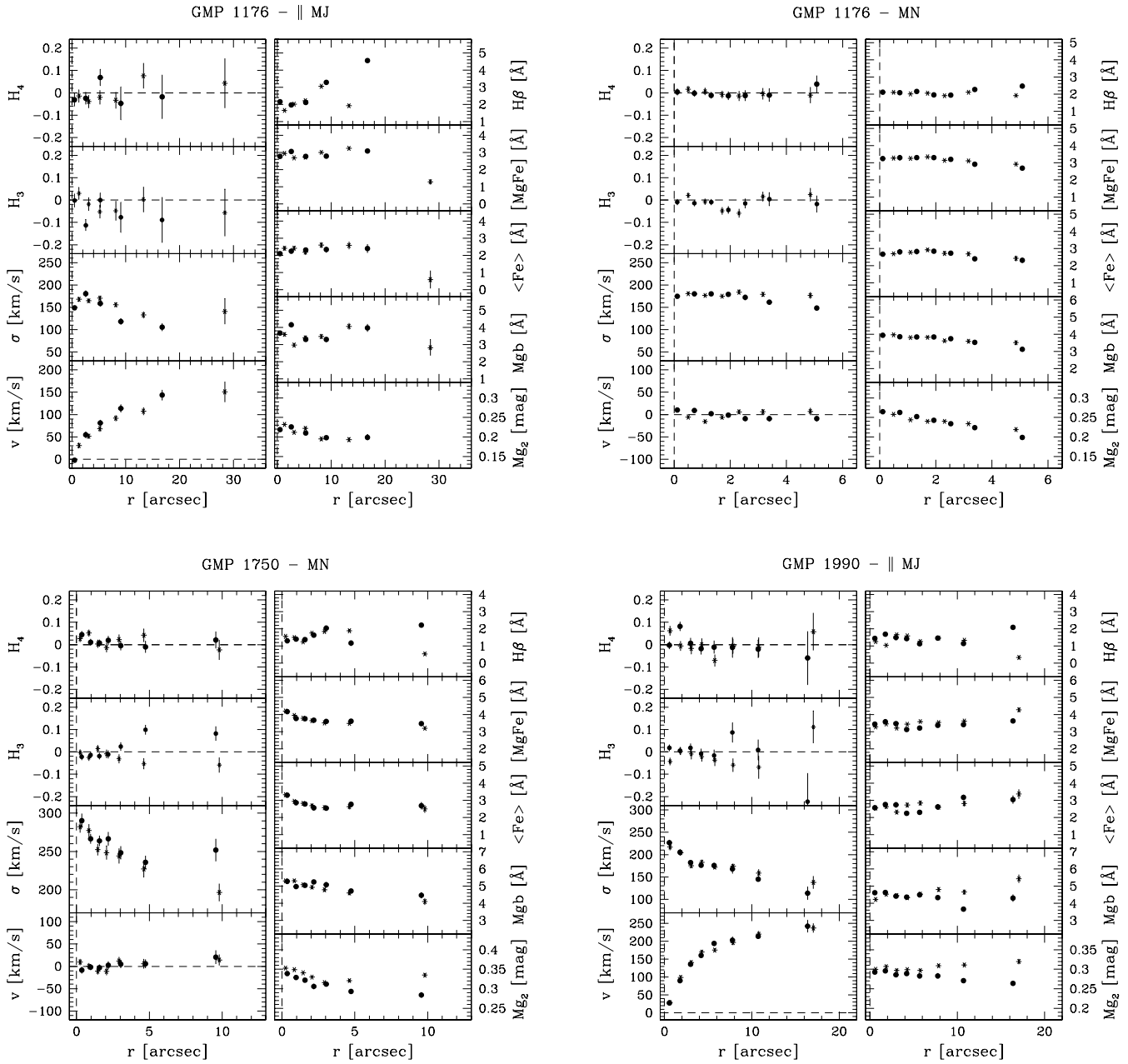
Fig. 2. continued.

all the measured indices for velocity dispersion broadening and calibrated our measurements to the Lick systems using stars from Faber et al. (1985). No focus correction was applied because atmospheric seeing was the dominant effect during observations (see Mehlert et al. 1998 for details). Errors on indices were derived from photon statistics and CCD read-out noise, and calibrated by means of Monte Carlo simulations. The measured values of Hβ, [MgFe], <Fe>, Mgb and Mg$_2$ are listed in Table 4 and plotted in Fig. 2.

Figure 3 shows the comparison between the measurements of Hβ, [MgFe], <Fe>, Mgb and Mg$_2$ along the major axis of GMP 1176 and GMP 3792 obtained here and measurements obtained in Paper I. The agreement within the error is excellent. The data we obtained in this paper are fully consistent with those of Paper I. Indeed, Fig. 4 shows that the mean cen-

tral values of σ, Hβ, [MgFe], <Fe>, Mgb and Mg$_2$ measured along the minor axes of the sample galaxies within an aperture of $2''$ and those obtained along the corresponding major axes are in agreement within the errors, assessing that the new galaxy dataset is on the Lick system.

5. Conclusions

We presented new radially resolved spectroscopy of 10 E and S0 galaxies of the Coma cluster. We derived rotation curves, velocity dispersion profiles and the H_3 and H_4 coefficients of the Hermite decomposition of the line of sight velocity distribution along the minor axis, the offset major axis and one diagonal direction. Moreover, we measured the line index profiles of Mg, Fe and Hβ line indices. The data complement
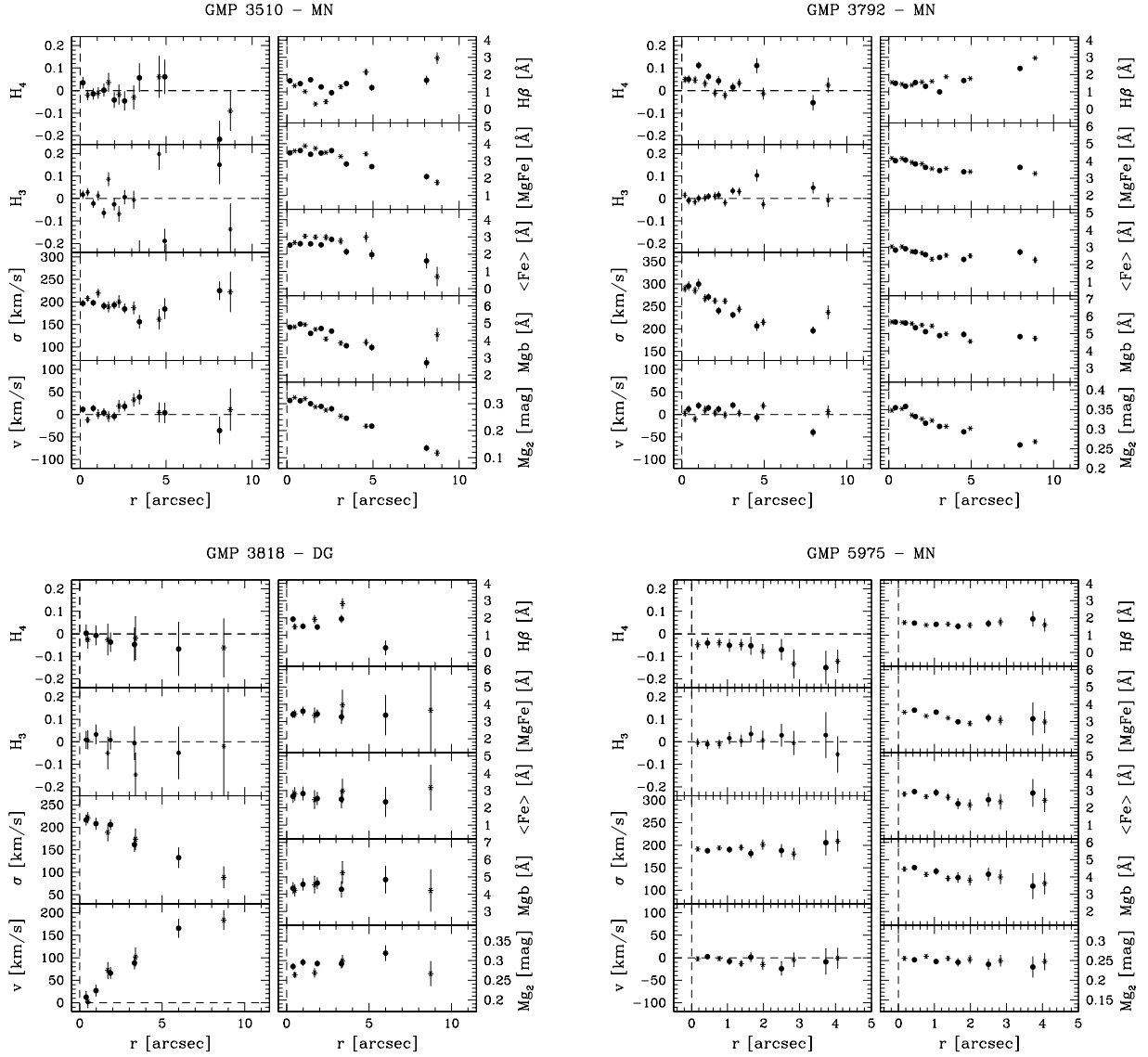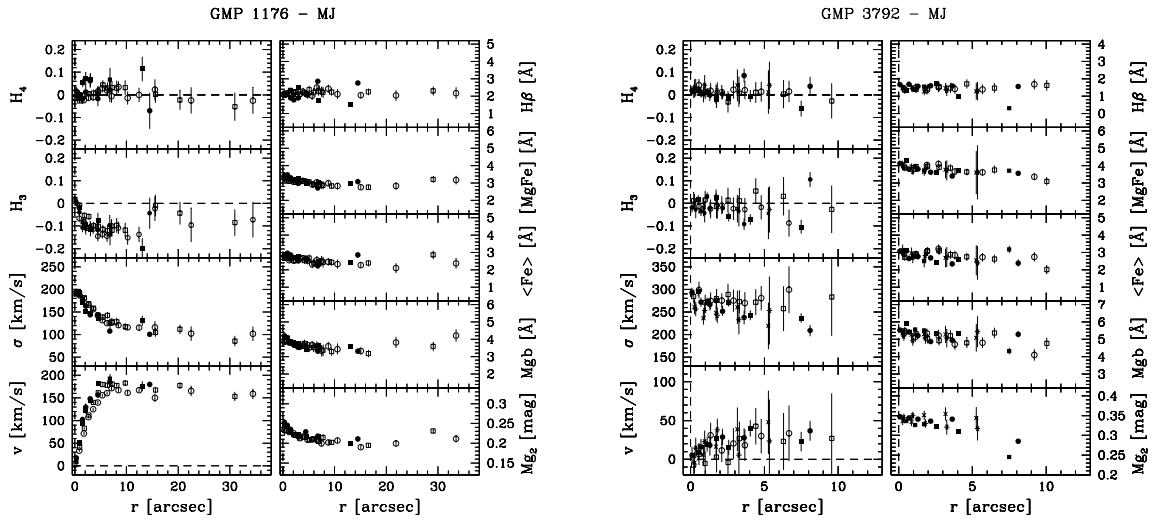
Fig. 2. continued.

Fig. 3. Kinematical parameters (v, σ, H_3, and H_4) and line indices profiles ($H\beta$, [MgFe], <Fe>, Mgb and Mg$_2$) along the major axis of GMP 1176 (left panels) and GMP 3792 (right panels) measured during run 1 (open symbols) and run 4 (asterisks) compared to those obtained by Mehlert et al. (2000, filled symbols). For each run different symbols refer to the different sides of the galaxy.
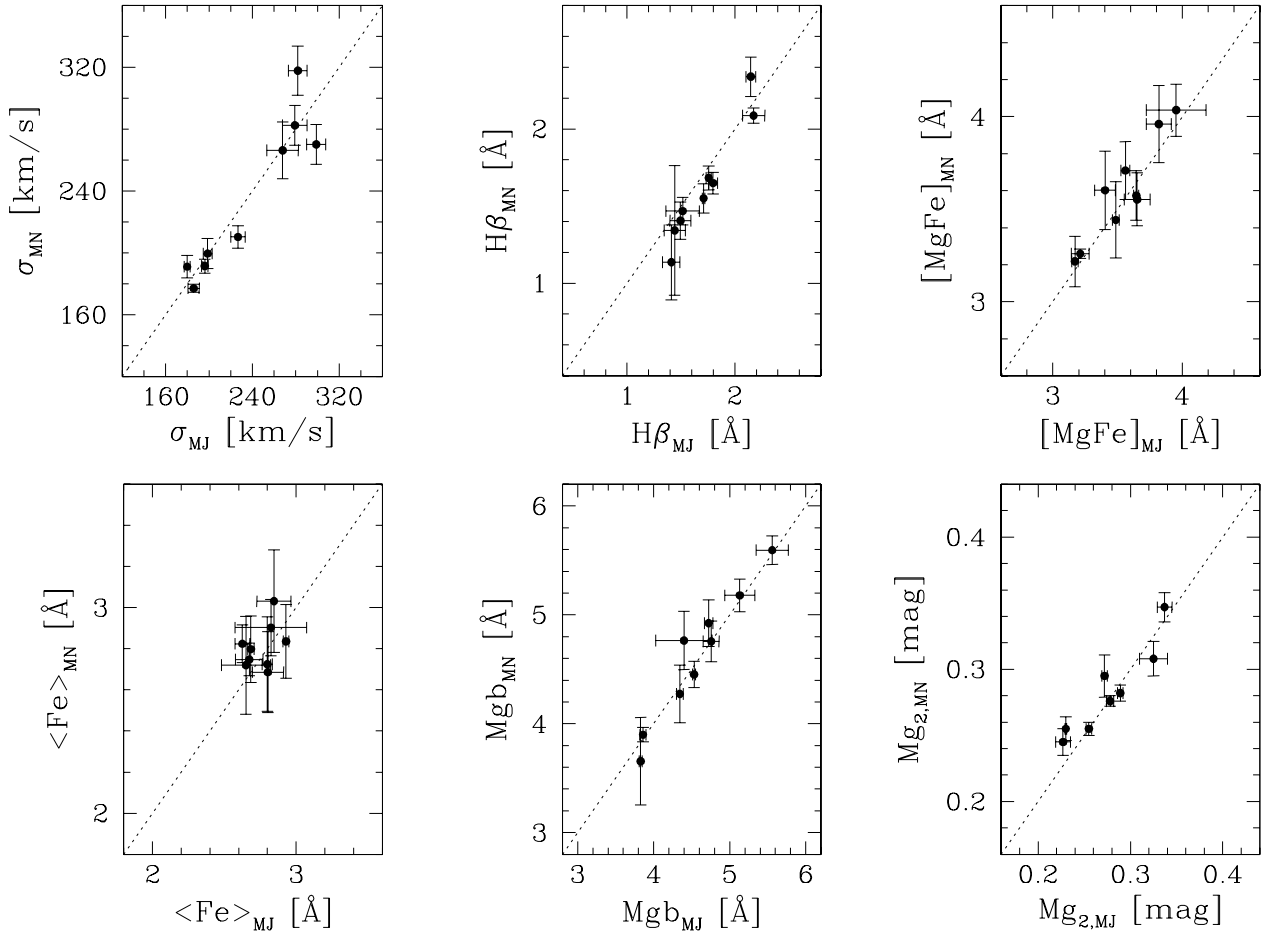
Fig. 4. Central values of σ, Hβ, [MgFe], <Fe>, Mgb and Mg$_2$ measured along major and minor axes and averaged within an aperture of 2″.

the existing set along the major axis and have a precision and radial extent sufficient to construct flattened and rotating dynamical models of the galaxies and study their radially resolved stellar populations. Future papers of this series will address these issues.

References

Bender, R. 1990, A&A, 229, 441

Bender, R., Saglia, R. P., & Gerhard, O. E. 1994, MNRAS, 269, 785 (BSG94)

Carter, D., Mobasher, B., Bridges, T. J., et al. 2002, ApJ, 567, 772

Davies, R. L., Burstein, D., Dressler, A., et al. 1987, ApJS, 64, 581

Faber, S. M., Friel, E. D., Burstein, D., & Gaskell, C. M. 1985, ApJS, 57, 711

Gerhard, O. E. 1993, MNRAS, 265, 213

Gerhard, O., Kronawitter, A., Saglia, R. P., & Bender, R. 2001, AJ, 121, 1936

Godwin, J. G., Metcalfe, N., & Peach, J. V. 1983, MNRAS, 202, 113

González, J. J. 1993, Ph.D. Thesis, University of California, Santa Cruz

Gorgas, J., Efstathiou, G., & Salamanca, A. A. 1990, MNRAS, 245, 217

Jørgensen, I., Franx, M., & Kjærgaard, P. 1995, MNRAS, 276, 1341

Jørgensen, I. 1999, MNRAS, 306, 607

Komiyama, Y., Sekiguchi, M., Kashikawa, N., et al. 2002, ApJS, 138, 265

Lucey, J. R., Guzmán, R., Steel, J., & Carter, D. 1997, MNRAS, 287, 899

Mehlert, D., Saglia, R. P., Bender, R., & Wegner, G. 1998, A&A, 332, 33

Mehlert, D., Saglia, R. P., Bender, R., & Wegner, G. 2000, A&AS, 141, 449 (Paper I)

Poggianti, B. M., Bridges, T. J., Carter, D., et al. 2001a, ApJ, 563, 118

Poggianti, B. M., Bridges, T. J., Mobasher, B., et al. 2001b, ApJ, 562, 689

Osterbrock, D. E., Fulbright, J. P., Martel, A. R., et al. 1996, PASP, 108, 277

van der Marel, R. P., & Franx, M. 1993, ApJ, 407, 525

Worthey, G., Faber, S. M., González, J. J., & Burstein, D. 1994, ApJS, 94, 687